British Journal of Civil and Architecture Engineering
ISSN: 2232-8232
Volume 02, Issue 06, June, 2020

A Corrosion Model for Prediction of the Service Life of Reinforced Concrete Water Conveyancing Structures.O

Philip Mogire[1*], Silvester Abuodha[2], John Mwero[3], Geoffrey Mang'uriu[4],

Department of Civil and Construction Engineering, University of Nairobi, Kenya[1,2,3]
Department of Civil, Construction and Environmental Engineering Jomo KenyattaUniversity of Agriculture & Technology, Nairobi, Kenya[4]

Corresponding author: 1*

ABSTRACT— With increased competing demands of sustainable and green structures to support the United Nations sustainable development goals, new technologies are evolving for efficient design and manufacture and construction of civil and environmental engineering products. Researchers have up scaled their effort to develop techniques to monitor the performance of civil engineering structures within their service life for optimum return from investment. The aim of this research was to develop a corrosion model for prediction of the service life of reinforced concrete water conveyancing structures. To achieve the desired objective, steel samples were cast in 9 cylinders each of 150mm diameter x 300mm long, 130mm diameter x 300mm long and 100mm diameter x 300mm long in concrete of characteristic strength 25/mm2,30N/mm2 and 35N/mm2 respectively. After 24 hours the cast specimens were demolded and immersed in curing tanks for 28 days and then immersed in a 3.5% industrial sodium chloride solution under 6V. The accelerated corrosion specimens were monitored for onset of cracks and stopped when the cracks were 0.2mm in width. The physical and chemical properties of the materials were investigated for compliance with relevant and applicable British and Kenyan standards for conformity to acceptable criteria. The concrete materials were batched by weight and mixed by a lab electric pan concrete mixer in batches of 0.009 m3. The concrete batches were tested for consistency by the slump and compaction factor tests. The applicability of existing models for critical corrosion depth for cover cracking was assessed. The corrosion current density of existing models was evaluated using results of this work and a model was proposed that matched with the experimental data reasonably well. Further, a corrosion service life prediction model that takes account of the cover to the rebar, the compressive strength and split tensile properties of concrete has proposed. The service life model developed here is for reinforced concrete water conveyancing structures subjected to chloride contamination. The model defines a criterion for corrosion initiation period, crack propagation period to 0.05mm width and propagation period from 0.05mm to 0.2mm. The results of the analysis of the present model significantly correlate well with experimental work and results of other researchers.

KEYWORDS: Service Life model, Corrosion, Reinforced Concrete.

1. INTRODUCTION

Among the materials used for construction of water conveyance structures is reinforced concrete due to its excellent performance and overall advantages. Corrosion of steel reinforcement has been recognized as a primary factor contributing to the deterioration of concrete structures [1,2]. Deterioration due to reinforcement corrosion leads to a decrease in durability of reinforced concrete structures resulting in a sharp reduction in their service lifespan and high maintenance costs [3]. The corrosion of steel reinforcement in concrete is an electrochemical process that causes the dissolution of iron to form a complex mixture of iron oxides,

hydroxides and hydrated oxides that evolves according to the prevailing local environment [4,5]. Corrosion products have specific volumes ranging from about two to six times that of the iron consumed [6] depending on the degree of oxidation. The main corrosion-induced damage mechanisms in reinforced concrete structures is shown by;
a decrease in the rebar cross-sectional area,
a possible loss of steel load capacity [7,8]
loss of flexural stiffness [9,10]
• cracking and spalling of the concrete cover [11,12]
• loss of bond along the steel/concrete interface [8].

Although most of the research on chloride-induced corrosion has been on chloride ingress into concrete, there has been an increasing effort in recent years to quantify the progressive damage in reinforced concrete due to the advancement of steel reinforcement corrosion [13-15]. The new effort is of great relevance in the structural assessment of deteriorated reinforced concrete water conveyancing structures with corroded reinforcement, and it must be included in estimations of the service life. Extensive analytical, numerical and experimental studies have been devoted to cracking of the concrete cover due to reinforcement corrosion. To speed up the corrosion process in the experiments, impressed current is adopted [16,17]. This provides corrosion of reinforcing steel bars, where the whole surface of the bar corrodes. Another method used to accelerate corrosion is immersing reinforced concrete samples in a chloride rich solution and connecting the reinforcing bar to cathode element through a particular voltage [18]. While in the beginning some pits on the reinforcement bar do occur, general corrosion is dominant at later stages [19]. Due to time constraints, concrete cracking due to natural chloride induced corrosion is rarely studied [20]. External chloride penetration leads to pitting corrosion, which creates non-uniform pressure around the bar. This could potentially lead to faster cover cracking than uniform corrosion. Analytical or numerical models based on the thick-walled cylinder theory; and numerical models based on finite elements or similar methods have also been devoted to studying the reinforced concrete corrosion phenomenon. Analytical and numerical models based on the thick-walled cylinder theory, with different levels of sophistication, have been used by a number of authors (e.g. [21,23]. The rate of corrosion is usually not constant but evolves due to the corrosion process itself and due to climate variations. Therefore, a representative, or average, value of the corrosion rate, (Vcorr.), first has to be determined 24]. The rate of corrosion (Vcorr.) in reinforced concrete can be represented by the volumetric loss of the reinforcement bars by unit of surface area and unit time and can be obtained from equation 1 or 2[25].

V_{corr} (mm/y) = 0.0116 i_{corr} (µA/cm^2) for uniform corrosion current 1)
or
V_{corr} (mm/y) = 0.0116 I_{corr} (µA/cm^2) for non-uniform corrosion current 2)
Where i_{corr}. is the uniform corrosion current density?
$\mathbf{I_{corr}}$. is the non-uniform corrosion current density?

Due to the impossibility of direct visual observation of the morphology of corrosion, I_{corr} is the most feasible expression of the corrosion current when measuring in concrete [25] and therefore equation 2 is preferred. For getting accurate rates of corrosion, it's essential that the values of the corrosion current density are obtained in order to accurately predict the service lifespan of the reinforced concrete structures [26]. I_{corr} is usually obtained through electrochemical measurement in an experiments [27,28]. The shortcomings of the electromechanical determination of Icorr include;

- I_{corr} is measured on the whole exposed area of the steel reinforcement; however, the corrosion is localized in a small zone.
- The measured I_{corr} value is significantly affected by the galvanic current flowing between the corroding and passive zones on the steel surface [29].

Due to the shortcomings of the electromechanical technique to measure Icorr., there is need to develop an accurate criterion for its measurement. The rate of reinforcement corrosion can also be calculated from the weight loss method in equation 3.

V_{corr} (mm/y) = 87.6 x (W / DAT) [30] 3)

Where
W = weight loss of the reinforcement bar in milligrams
D = Reinforcement bar density in g /cm^3
A = Surface area of the sample exposed to corrosion in cm^2
T = time of exposure of the reinforcement bar in hours

This research presents a service life model for reinforced concrete water conveyancing structures. The validity, accuracy, and efficiency of the proposed model is established by comparing the model results with experimental work and works of other researchers. The results of the analysis of the present model significantly correlate well with experimental work and results of other researchers.

2. BACKGROUND OF CORROSION KINEMATICS

The electrochemical process that underlies corrosion of steel reinforcement in concrete involves two chemical reactions. The anodic reaction is iron oxidation, described by equation 4. Iron ions (Fe^{2+}) dissolve into the pore solution with electrons left inside the steel bar. These electrons are consumed by a cathodic reaction, i.e., an oxygen reduction producing hydroxides according to equation 5.

Anodic reaction:

$Fe \rightarrow Fe^{2+} + 2^{e-}$ 4)

Cathodic reaction

$O_2 + 2H_2O + 4^{e-} \rightarrow 4OH^-$ 5)

Both the anodic and cathodic reactions occur along the surface of the steel electrode. Additionally, an ionic current of hydroxide ions flows through the surrounding electrolyte from the cathodic to the anodic areas, balanced by an electric current through the steel, as shown in Fig. 2.1[31]. The anode hydroxide ions and Fe2+ ions form ferrous hydroxide, the primary corrosion product, which undergoes further oxidation, becoming black rust or brown rust depending on the amount of oxygen available.

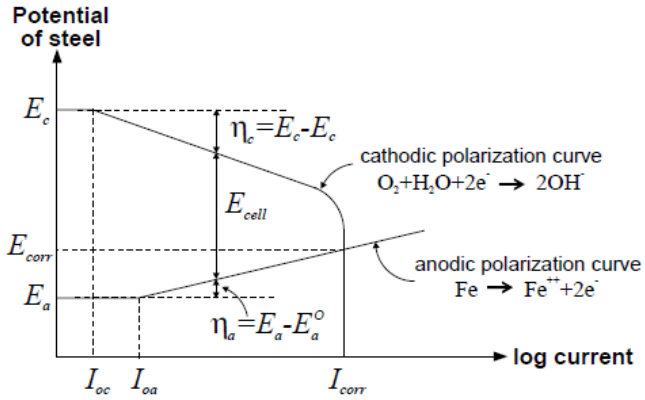


Figure 2.1 Evans diagram for the anodic and cathodic processes taking place on the reinforcing steel surface. [31]

2.1 Reinforcement corrosion

Assuming an electric charge and isotropic conductivity, the electric potential distribution between the anodic and cathodic polarization curve is described by Laplace's Equation 6 whose solution can only be derived with prescribed geometries and boundary conditions.;

$$\nabla^2 E = 0 \qquad 6)$$

Where ∇^2 is the Hamilton operator

E is the Electric potential

The current density at any location of the steel surface can also be determined by Ohm's law from Equation 7.

$$i_{corr.} = \frac{1}{\rho_{el}} \frac{\partial E}{\partial n} \qquad 7)$$

Where ρ_{el} is the concrete resistivity

n is the direction normal to the steel surface.

Taking into account the effects of activation and concentration polarization according to Butler-Volmer kinetics, the surface boundaries can be described by the Tafel Equations 8 and 9.

The kinetics of oxidation of iron are given by:

$$i_a = i_{oa} e^{2.3(E_a - E_{oa})/\beta_a} \qquad 8)$$

The kinetics of oxygen reduction are given by:

$$i_c = \frac{C}{C_o} i_{oc} e^{2.3(E_{oc} - E_c)/\beta_c} \qquad 9)$$

Where

i_a= Current density of the iron oxidation reaction (µA/cm^2)

i_{oa}= Exchange current density for iron dissolution (µA/cm$^{2)}$

E_a= Potential at the concrete pore solution immediately next to the steel surface(V)

E_{oa}= Equilibrium potential of the anodic reaction (V)

β_a = Activation tafel slope for the anodic reaction (V)

i_c = Current density of the oxygen reduction reaction (µA/cm^2)

i_{oc} = Exchange current density for cathodic reaction (µA/cm$^{2)}$

E_{oc} = equilibrium potential of the cathodic half-cell reaction, taken as the standard electrode potential, i.e., 0.160 V vs. SCE

E_c =potential at the concrete pore solution immediately next to the steel surface(V)

β_c = Activation tafel slope for the Cathodic reaction (V)
C_o=dissolved oxygen concentration at the external concrete surface (kg/m^3 of solution)
C = issolved oxygen concentration at the steel surface (kg/m^3 of solution)
It has been observed that β_a increases over time when chloride ions are present in the concrete, from 0.338 V at 1 day to 0.480 V at 90 days while β_c decreases over time from 0.309–0.394V over the same period and condition. [32].
The reinforcing steel is freely corroding when the polarization taking place at the anode and the cathode is enough to make their polarization curves meet as illustrated in Fig.2.2. At this point, the corrosion system develops a new equilibrium corrosion potential E_{corr} and corrosion current I_{corr}. The intersection of the two electrode polarization curves represents conditions at which the anodic and cathodic currents are equal (but opposite in polarity) and no net current flows across the steel/concrete interface, i.e.,

$$I_{corr} = i_a \, x \, A_a = i_c \, x \, A_c \quad 10)$$

where A_a and A_c denote the surface areas where the anodic and cathodic reactions take place, respectively. By substituting Eqs. 8 and 9 into Equation 10 an estimate of the equilibrium corrosion potential can be obtained from equation 11:

$$E_{corr} = \frac{1}{\beta_a+\beta_c}\left[\frac{\beta_a \beta_c}{2.3} \, ln\left(\frac{i_{oc}}{i_{oa}} \frac{C}{C_o} \frac{A_c}{A_a}\right) + \beta_c E_{oa} + \beta_a E_{oc}\right] \quad 11)$$

Taking into account the effects of resistivity and oxygen diffusion, and assuming a relative humidity of 75 % and temperature of 20^{O}C, Vu and Stewart [33] developed an empirical model which gives the corrosion current density at the start of the propagation period (at time t_1) as a function of water cement ratio and cover thickness:

$$i_{corr}(t_1) = 37.8(1 - w/c)^{-1.64}/d \quad (\mu A/cm^2) \quad 12)$$

where *w/c* is the water cement ratio obtained from the Bolomey's formula and *d* is the cover thickness (mm).
For t < 1 year

$$i_{corr}(t_2) = \left[i_{corr}(t_1)(1 + t_2)^{\frac{-1}{3}}\right] /d \quad (\mu A/cm^2) \quad 13)$$

Inserting equation 12 into Equation 13 gives:

$$i_{corr}(t_2) = \left[37.8\,(1 - w/c)^{-1.64}(1 + t_2)^{\frac{-1}{3}}\right] /d \quad (\mu A/cm^2) \quad 14)$$

For t > 1 year

$$i_{corr}(t_2) = [i_{corr}(t_1)0.85\, {t_2}^{-0.29}] /d \quad 15)$$

Inserting Equation 12 into 15 gives

$$i_{corr}(t_2) = [32.13\,(1 - w/c)^{-1.64}\, {t_2}^{-0.29}] /d \quad 16)$$

Li 2004a [34] proposed a corrosion density model in equation 17,

$$i_{corr} = 0.3682 \ln(t) + 1.1305 \quad 17)$$

Where i_{corr} is the corrosion current density (μm/cm^2) and t is the time (years) from corrosion initiation.
The corrosion model was established from the experimental data and the influence of the corrosion duration was considered. This model cannot rationally reflect the corrosion process of the reinforcement bar in chloride induced corrosion affected reinforced concrete structures as other factors influencing the corrosion rate are ignored.

2.2 Service life design

The Tuutti's model [35] is widely accepted as the conceptual model for the deterioration of structures (Fig.2.2). As a function of time, the model distinguishes an initiation time followed by a propagation time and shows the respective limit states in the two periods.

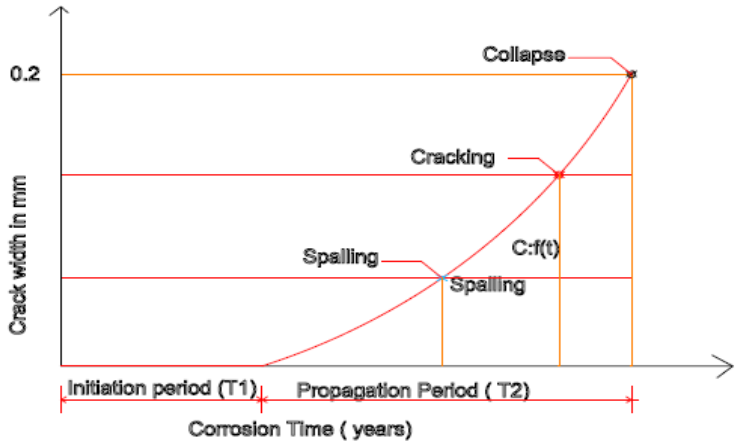


Figure 2.2: Graph of Service life design limit states for water structures

From the graph in figure 2.3

$T_{cr} = T_1 + T_2$ 18)

2.2.1 Initiation time T_1

The time needed for first cracking of the concrete cover as a result of the expansive forces exerted by the corrosion products mainly depends on the tensile strength of the concrete(f_t), the type of corrosion, the rate of corrosion and the concrete cover-to-rebar diameter ratio c/d which define the critical penetration depth.

Rasheeduzzafar et al. [36] found that the ratio of concrete cover to bar diameter was a better predictor for critical corrosion loss than either parameter alone.

Based on experimental studies, Rodriguez et al. [15] proposed Equation 19 for evaluating the attack penetration x_{crit} corresponding to crack initiation:

$x_{crit} = 83.8 + 7.4\frac{c}{d} - 22.6f'_t$ (μm) 19)

where

x_{crit} is the attack penetration or the decrease in the reinforcing bar radius (μm),

c/d is the cover/diameter ratio and

f'_t t is the concrete tensile strength N/mm^2).

From Equation 19 the critical penetration depth increases with cover depth and decreases with increasing reinforcement diameter, which is as reported in most experimental investigations. However, as the resistance of the concrete to cracking is strain-limited and not strength-limited the concrete tensile strength may not be the main parameter controlling the crack initiation. Moreover, in the relationship the unit is not correct, indicating that the tensile strength should be replaced or combined with other mechanical concrete parameters [37].

Xu and Shayan [38] considered the combination of concrete cover and its embedded steel as a thick-wall concrete cylinder which surrounds the embedded steel, and the expansion of corroded steel exerting an internal pressure to the concrete cylinder. They derived Equation 20 for the attack penetration depth x_{crit}.

$x_{crit} = \frac{f_t(c+d)(1+\nu)}{E_{eff}d\beta}$ 20)

Where,

x_{crit} = Corrosion loss at crack initiation(μm)

C= Concrete cover (mm)

d= bar diameter(mm)

f_t = Concrete tensile strength (N/mm^2)

ν =concrete poison's ratio

β = Relative volume change due to conversion of steel to rust $= \left({}^{\Delta V}/_{V}\right)$

E_{eff} =effective elastic modulus=E/(1+ϕ) (N/mm^2)

E =Elastic modulus (N/mm^2)

ϕ = concrete creep coefficient

From their model, the predicted critical corrosion loss was found four or greater as much as the calculated values based on the measured corrosion rates from Linear Polarization Resistance (LPR) test in their research. This is because in calculating corrosion loss from the LPR test, it is assumed that the whole surface area subjected to corrosion is corroding. This is not true for non-uniform corrosion and therefore the calculated corrosion loss from LPR tests should be modified based on the actual corroded area of the embedded steel to present the real values.

Torres and Sagues [39] studied the effects of localized corrosion and derived Equation 21 which relates the length of corroded steel and cover-bar diameter ratio to the critical corrosion loss.

$$x_{crit} = 11.0\ \frac{c}{d}\left(\frac{c}{l}+1\right)^2 \qquad 21)$$

Where

x_{crit} = Corrosion loss at crack initiation(µm)

C= Concrete cover (mm)

d= bar diameter(mm)

l= length of exposed steel (mm)

Other factors including the tensile strength that may contribute to the critical penetration depth were not taken into account in Equation 21. The initiation corrosion period is evaluated from Equation 22:

$$T_1(years) = \frac{x_{crit}(mm)}{V_{corr}\left(\frac{mm}{year}\right)} \qquad 22)$$

2.2.2 Propagation time T_2

The corrosion propagation period (T_2) is the time necessary for sufficient corrosion to occur to cause unacceptable damage to the reinforced concrete structures, e.g. cover cracking. The length of this period depends on the definition of an acceptable limit state [40]. This level of damage will vary depending on the requirements of the use of the structure. Assuming a particular damage limit state, the propagation period depends principally on the corrosion rate. The limit state may be described in terms of parameters that define the propagation period including loss of steel cross sectional area [41] and loss of steel/concrete bond [42]. Once the corrosion rate (V_{corr}) is quantified, the effect of any variable that alters it during propagation period [43], such as inhibitors or the presence of moisture in chloride-bearing concrete, can be studied, the condition of a real structure can be assessed, and the propagation period [44] quantified by integrating the value over time. Based on theoretical physical models for corrosion of steel in concrete exposed to seawater, Bazant et al. [45] proposed a numerical model shown in Equation 23 for reinforcement corrosion in concrete, to assess the time to corrosion that may lead to splitting of cover concrete.

$$T_2 = \rho_{corr}\frac{d\Delta d}{pj_r} \qquad 23)$$

Where

T_2 = propagation period (years).

ρ_{corr} =Combined density factor for steel and rust (kg/m^3)

d =diameter of rebar(mm)

Δd =increase in diameter of rebar due to rust formation(cm)
P = perimeter of rebar(mm)
j_r = instantaneous corrosion rate of rust (g/m^{2}s)
The instantaneous corrosion rate of rust can be calculated from Equation 24;

$$j_r = \frac{W}{F} i_{corr} \quad 24)$$

Where
W=equivalent weight of steel (g)
F= Faradays constant(C)
i_{corr} =Corrosion current density (µA/cm^2)
From Bezant's numerical model, the corrosion rate is the most significant parameter in determining the time to cracking of the cover concrete. This model has never been experimentally validated.
Liu and Weyers [18] derived a model that includes the time required for corrosion products to fill an assumed porous zone at the steel/concrete interfaces before creating an internal pressure on the surrounding concrete. In their model (Equation 25), the time from corrosion initiation to cover cracking, t_{crack}, is given as a function of the critical amount of rust product needed to induce cracking of the concrete cover, M_{crit}, and the corrosion rate, k_p:

$$T_{crack} = \frac{M^2 crit}{2k_p} \quad 25)$$

Where M_{crit} is modelled as Equation 26;

$$M_{crit} = \rho_{rust} \left(\pi \left[\frac{C f_t}{E_{ef}} \left(\frac{a^2+b^2}{b^2-a^2} + v_c \right) + t_1 \right] d + \frac{M_{st}}{\rho_{st}} \right)$$

26)
v_c is Poisson's ratio of the concrete,
E_{ef} = an effective elastic modulus of the concrete; $E_{ef} = Ec/(1+\varphi)$
E_c = elastic modulus of the concrete (N/mm^2)
a = the inner radius [$(d+2t_1)/2$] (mm)
b = the outer radius [$C+(d+2t_1)/2$] (mm)
C = the concrete cover (mm)
Ec = elastic modulus of the concrete
φ= the creep coefficient of the concrete
t_1 = is the thickness of the concrete under pressure(mm)
d = original diameter of steel (mm)
f_t = Split tensile strength(N/mm^2)
Equation 27 shows Liu and Weyers expression of the rate of rust production, k_p:

$$k_p = 0.098\ x\ 10^{-4}(1/\alpha)\pi d i_{corr} \quad 27)$$

where:
0.098 = numerical coefficient to fit experimental data
α = relation between atomic weight of iron (55.8) and the molecular weight of the rust product; e.g $\alpha = 0.523$ if the corrosion product is $Fe(OH)_3$
d = diameter of the steel bar (mm)
i_{corr} = annual mean corrosion rate (µA/cm^2)
Inserting Equation 26 and 27 into Equation 25;

British Journal of Civil and Architecture Engineering
ISSN: 2232-8232
Volume 02, Issue 06, June, 2020

$$T_{crit} = \left[\rho_{rust}\left(\pi\left[\frac{Cf_t}{E_{ef}}\left(\frac{a^2+b^2}{b^2-a^2}+v_c\right)+t_1\right]d+\frac{M_{st}}{\rho_{st}}\right)\right]^2\frac{5.846\alpha}{di_{corr}} \quad 28)$$

For a given crack width (w)[18],Equation 29 can be used to evaluate the rebar radius decrease

$$w = 0.05 + \beta[x - x_{crit}], [0 \le w \le 1.0mm] \quad 29)$$

Where

w=characteristic crack width(mm)

x=rebar radius decrease(mm)

x_{crit}=critical penetration depth (mm)

β= Coefficient which depends on the position of the bar (β= 0.01 for top cast bars and 0.0125 for bottom cast bars

In Liu-Weyers model the rate of steel mass loss caused by corrosion was assumed to decrease with time in which the coefficients used were obtained by fitting experimental data. The thickness of the pore band around the steel/concrete interface(t_1) was assumed as 12.5 μm in the validation of their model. In good quality concretes the thickness of the concrete under pressure(t_1) is not a distinct band, the reported thickness varies, but is typically in the range of 15-50 μm [46-48]. The sensitivity of this parameter has not been studied. The model has not been verified against concrete structures under field exposure where chloride ions diffuse into the concrete. From Liu-Weyers model, T_2 can be found by subtracting T_1 from $T_{crack.}$

Based on field and laboratory data, Morinaga [49] suggested Equation 30 for predicting the time to cracking. He assumed that cracking of concrete will first occur when there is a certain quantity of corrosion products forming on the reinforcement.

$$T_2 = \frac{Q_{cr}}{j_r} \quad 30)$$

$$Q_{cr} = 0.602d\left(1+\frac{2c}{d}\right)^{0.85} \quad 31)$$

Where

Q_{cr} =amount of corrosion in concrete cracks(g/cm^2)

c = concrete cover thickness(mm)

According to Equation 30 the time to cracking is a function of the corrosion rate, concrete cover depth and reinforcing diameter. This model does not include any effect of mechanical concrete properties and it is difficult to identify the limitations of its validity.

Wang and Zhao [50] recommended a stage technique for utilizing limited component examination to focus the thickness of the corrosion product comparing to the time term when the surface concrete cracks. Their model is described in Equations 32-34;

$$T_2 = \frac{H}{p_r} \quad 32)$$

and

$$\frac{\Delta}{H} = 0.33\left(\frac{d}{c}\right)^{0.565} f^{1.436}{}_{cu} \quad 33)$$

$$p_r = \frac{W}{F\rho_{st}} i_{corr} \quad 34)$$

Where

W = equivalent weight of steel (kg)

f_{cu} = cube strength of concrete(kN/cm^2)

Δ = thickness of corrosion product (cm)

H= no of cracks in the cover

ρ_{st} =density of steel(kg/m^2)

i_{corr} is the average corrosion rate ($\mu A/cm^2$),
Wang and Zhao empirical model assumed that the corrosion products will fill the steel/ concrete interface and develop an expansive pressure or tensile stress on the cover concrete, which will crack when the exerted tensile stress from the expansive corrosion product exceeds the tensile strength of the concrete. This model is applicable when field and laboratory data for corrosion current density is available.

2.2.3 Service life of reinforced concrete water conveyancing structures

The end of service life of this research is limited by the maximum crack width allowed for water structures. In reference to BS 8007 cracks less than 0.2 mm in width will self-heal if the cracked concrete element is in contact with water that is not flowing or exerting a pressure.

Figure 2.3 [51] the relationship of the crack width and the wall thickness –water retaining height ration by

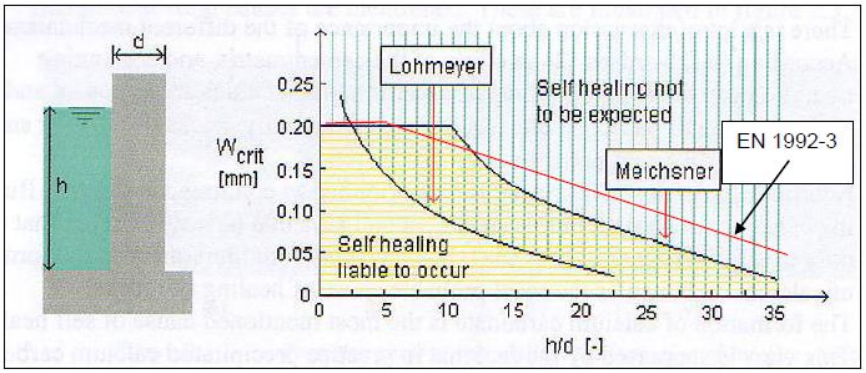


Figure 2.3: Self-healing of cracks to Jones [51]

From the graph in Figure 2.3 the Eurocode has h/d ratios higher than those by Lohmeyer and Meichner for crack widths less than about 0.17 mm. This shows that that for a given water height, h/d, and section thickness, h, EN1992-3 predicts that self-healing of cracks will occur at a larger crack width limit for crack widths less than 0.17 mm for a given hydraulic ratio. In this research due to consideration of water structures, a limit crack width of 0.2mm will be considered for low pressure reinforced concrete water structures. A number of modelling efforts have also been devoted to define the corrosion initiation and propagation periods but none has distinctively defined the periods for water conveyancing structures. The present work addresses two important aspects regarding the service life of reinforced concrete water conveyancing structures. The parameters for the initiation and propagation period are defined and the periods calculated. From the results a parametric study is done and a new proposed model for the service life of water conveyancing structures is defined.

3.Methodology

This study was conducted at the University of Nairobi Concrete and Materials Lab where the physical properties of the materials, sample preparation and testing were done. The chemical properties of the ordinary Portland cement and chloride content was done at the State Department of Infrastructure in the Ministry of Transport, Infrastructure, Housing and Urban Development of the Government of Kenya.

3.1 Concrete samples

The constituent materials for preparing test samples consisted of Ordinary Portland cement ($42.5N/mm^2$), clean river sand,20mm maximum size coarse aggregate and potable water.

3.1.1 Cement

The chemical composition of the cement used in this research was tested. Available cements in Kenya are manufactured in accordance to KS EAS 18-1: 2001, an adoption of the European Norm EN 197 cement standards [52]. The cements locally available are produced for specific uses [53]. The Cement used for this research was sourced from one wholesaler.

3.1.2. Other concrete constituents

Table 3.1 shows the description and source of other constituents of concrete used in the research.

Table 3.1. Details of materials used in the research

SN	Description	Source	Remark
1.	Fine aggregates	Stockpile vender sourced from Machakos River	This was washed and oven dried before use.
2	Coarse aggregates	Kenya builders quarry	5-20mm uniformly graded at source
3.	10mm ribbed bars	Local manufacturer	Factory cut to 400mm
4.	Mixing water	Potable water in the Lab	
4.	Mixing water	Potable water in the Lab	

3.2 Concrete Mix Design

With a characteristic strength of 25N/mm^2, 30N/mm^2 and 35N/mm^2 the concrete used was designed in accordance with the British Department of environment (DoE) method [54-55].

3.3 Accelerated Corrosion

3.3.1 Materials and Specimens

This was done through an impressed corrosion test using the procedure below;

i)10mm diameter x 400mm long ribbed bars were polished with abrasive papers.

ii) 120 mm of the surface length of each bar were sprayed with a zinc rich coating and left to naturally dry.

iii) The mixed concrete was poured into 9 cylindrical samples of 150mm diameter and 300mm long, 130mm diameter and 300mm long, 100mm diameter and 300mm long each with a 10mm diameter rebar

iv) The specimens were mechanically vibrated for 60s. After 24 hours, the cylindrical concrete specimens were demolded and cured for 28 days.

vi) The test specimens were dried for 24 hours and then subjected to accelerated corrosion by storing them in a tank containing 3.5 % NaCl at room temperature and an impressed voltage of 6Volts applied through a DC power supply regulator. The top and bottom surfaces of the concrete specimens were also sealed with Zinc

rich coating so as to allow only chloride ingress from the sides to simulate the corrosion of a section of a typical structural member in a water conveyancing structure.

3.3.2 Testing Methodology

The accelerated corrosion set up is shown in Fig.3.1. The rebars projecting were connected in series to the anode and the stainless steel rod was connected to the negative terminal (cathode). The test specimens were subjected to a constant voltage of 6 V applied to the system using a DC power supply regulator. The variation in development of corrosion current was monitored at regular intervals using a high impedance multimeter and the average for the corrosion period taken for calculation of the average mass loss.

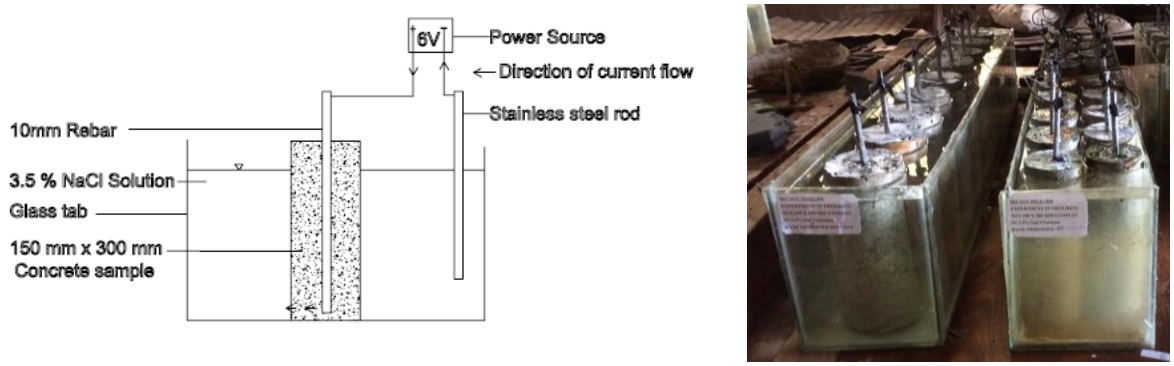


Figure 3.1: a) Schematic drawing of accelerated corrosion set up, b) Photo of the samples during experimentation

The appearances of first visible cracking were detected by visual observation using a magnification glass with power of x1000. The data collected for crack propagation provided the timing of first cracking and the subsequent time-dependent increase in crack width. After testing, the weight loss of bars due to corrosion were studied by cleaning, drying and weighing the reinforcement bars according to the gravimetric weight loss method as specified by Standard Practice for Preparing, Cleaning, and Evaluating Corrosion Test Specimens (ASTM G1 – 90). Fig.3.2shows samples during experimentation and measurement.



a) b) c) d) e)

Figure 3.2: a) Samples during experimentation b) sample with 0.2mm longitudinal crack c) crack measurement d) recovering the corroded steel and e) cleaned rebar's for gravimetric weight loss measurement.

3.4 Results of the material properties

i) Properties of aggregates

Various tests were carried out on the aggregates to determine their suitability for the research. Water soluble chlorides ions percentage were found to be zero in fine aggregates, 0.002 % in coarse aggregates all less than

0.03% acceptable in compliance with BS EN 12620: 2002.Table 3.2 shows the physical properties of the aggregates used in the study.

Table 3.2: Physical properties of aggregates used in the study

Material	Specific gravity	Absorption %	Silt content %	Max Size
Fine aggregates	2.6	1.8	7.4	4.0
Coarse aggregates	2.6	0.3	0	20.0

The specific gravity of all the aggregates are within the limits of 2.4 – 3.0 stated in literature [56,57] and they influence the mix design of the concrete. The water absorption of the fine aggregates is within the limits of 1% – 3% stated in the literature and British Standards [58-62] and therefore a low water absorption and hence suitable for concrete works. The very low water absorption in the coarse aggregates need was taken into consideration in the mix design. ASTM C117[63] gives an allowable limit of 10% for silt and clay content in fine aggregates for concrete production while BS 882 give a limit of 4% [64]. As a thumb rule according to [65], the total amount of deleterious materials in aggregates should not exceed 5%. The silt content in the fine aggregate was more than the allowable percentage of silt content, it was washed and oven dried before use. Table 3.3 shows the mechanical properties of the coarse aggregates used in the study.

Table 3.3: Mechanical properties carried on coarse aggregates.

Test	Size of aggregates mm	Crushing value %	Impact Value %	Flakiness index %	Loss Angeles Abrasion Value %
Result	5-20	18	8	35	20

The mechanical properties of aggregates cannot be improved but depend on the properties of the parent rock. The Aggregates Impact Value is less than 30% value stated in literature and British Standards [65] and specified in [66]. It therefore follows that Aggregates Impact Value of all the aggregates tested are very suitable for concreting works. The Aggregate Crushing Value is less than 35% value allowed for concreting works as stated in the literature [67].

ii) Chemical Properties of Cement used in the research

Table 3.4 shows results of the chemical composition of the cement used in the research. All the constituents of cement oxides were within the acceptable limits.

Table 3.4 Result of Chemical composition the Cement used.

SN	Test	Result of the sample	KS EAS 18-1: 2001 Requirement
1.	CaO%	59.11	Sum ≥ 50
2.	SiO_2%	21.56	
3.	SO_3%	2.78	≤ 3.5
4.	MgO%	1.04	≤ 5
5.	K_2O%	0.051	
6.	Fe_2O_3%	3.48	
7.	Al_2O_3	8.09	3-8
8.	Na_2O_3%	0.018	
9.	LOI%	0.10	≤ 5
10.	Cl%	0.016	≤ 0.1
11.	IR%	0.55	≤ 5

a) Effect of sum of lime (CaO) and silicon dioxide (SiO_2) corrosion

The sum of lime (CaO) and silicon dioxide (SiO_2) in the chemical analysis of ordinary Portland cement sample was 80.67% ≥ 50% within the acceptable limit [66]. This is consistent with the known fact that both CaO and SiO_2 give strength to concrete though SiO_2 has to be limited relative to CaO in order not to negatively affect setting time. The rate of corrosion is related to the strength of a concrete sample while reduced setting time minimizes plastic shrinkage cracking and hence the rate of corrosion.

b) Effect of CaO/SiO_2 on corrosion

The ratio of lime (CaO) to silicon dioxide (SiO_2) contents in ordinary Portland cement should be greater than 2. The restriction on the ratio of lime to silicon dioxide [66] is to ensure that the quantity of silicon dioxide is considerably lower than that of lime so that the setting of concrete is not inhibited minimizing plastic shrinkage cracking and hence limiting corrosion.

c) Effect of MgO on corrosion

The quantity of magnesium oxide (MgO) in ordinary Portland cement should not exceed 5% [66]. If the quantity of MgO is in excess of 5 percent, cracks will appear in concrete and which may affect the rate of corrosion by generating spots for penetration of chloride ions in concrete.

d) Effect of SO_3 on corrosion

The quantity of sulphur trioxide (SO_3) content in ordinary Portland cement was less than 3.5 % as required. SO_3 reduces the rate of the passive layer dissolution inhibiting the onset of corrosion.

e) Effect of Chloride Content on corrosion

The chloride content in ordinary Portland cement was less than 0.4% as required. Chloride ions in aqueous solution destroys the passivation film of rebars in the process of competing with hydrogen and oxygen ions in the adsorption process, thus leading to the occurrence of pitting corrosion, hole corrosion and crevice corrosion.

f) Effect of Al_2O_3 on corrosion

British Journal of Civil and Architecture Engineering
ISSN: 2232-8232
Volume 02, Issue 06, June, 2020

Aluminium oxide (Al_2O_3) reacts with free lime in concrete to form $CaAl_2Si_3O_{12.}$ which reduces the permeability of chloride and improving the corrosion resistance property of embedded steel in concrete. Above 8% the Al_2O_3 will be in an active condition reducing the corrosion resistance.

g) Effect of Fe_2O_3 on corrosion

Iron oxide (Fe_2O_3) contributes to cement colour and helps in the fusion of the different ingredients. Fe_2O_3 forms the passivation film reducing the oxygen diffusion rate, which, in turn, reduces the **corrosion** rate.

h) Effect of Residues on corrosion

British standards consider Na_2O, K_2O, TiO_2 and P_2O_5 in ordinary Portland cement as residues and limit the sum of all of them to 5%. If in excess of 5% efflorescence and unsightly cracking will occur aggravating corrosion.

iii) Gradation of Coarse and Fine aggregates

Particle size distribution analysis on a representative sample shown on Fig.3.3 for the course aggregates for the work was carried out to obtain the proportions by weight of the different sizes of coarse aggregates present. The sample is well graded with a maximum aggregate size was 20mm.

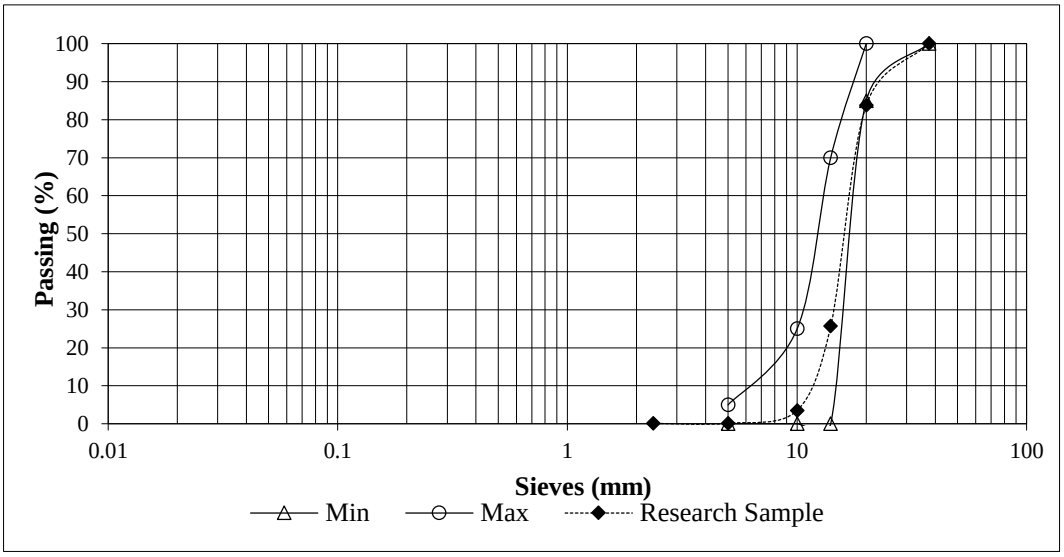


Figure 3.3: Graph 1 Gradation of Coarse aggregates

Particle size distribution analysis as shown on Fig.3.4 on a representative sample of the fine aggregates for the research was carried out to obtain the proportions by weight of the different sizes of fine particles present according to BS 812-103 and BS 882. The proportions were expressed as percentages by weight passing various sieve sizes conforming to BS 410. As shown on the graph of Fig.3.4, the coarse aggregates were well graded and expected to give a well interlocked composite concrete mix.

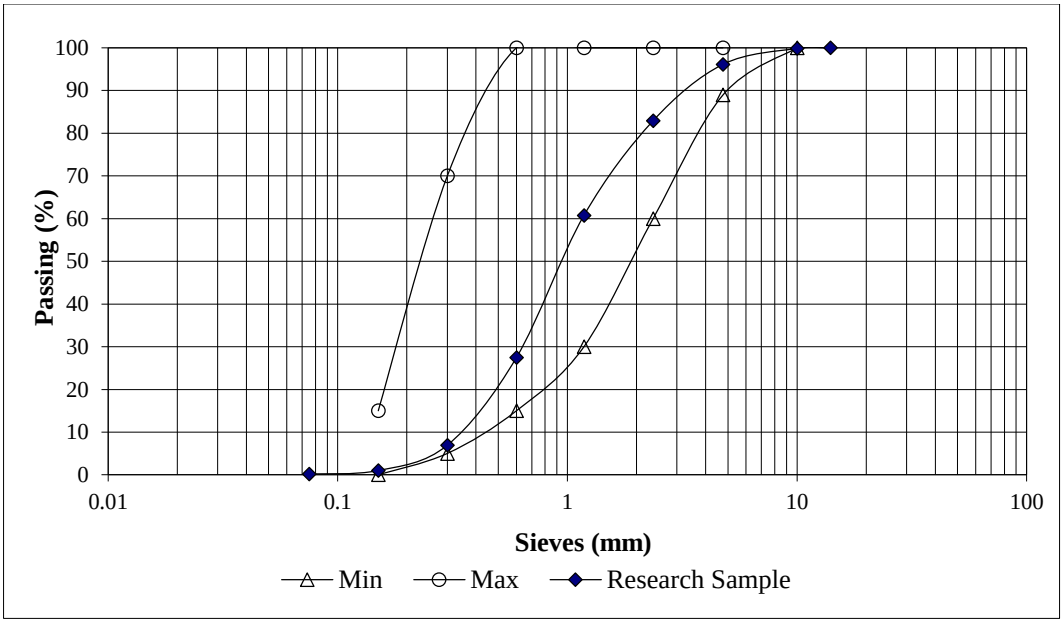


Figure 3.4: Graph of gradation of fine aggregates

iv)Results of hardened concrete

Table 3.5 shows a parametric study of the results of hardened concrete while Table 3.6 show a statistical analysis of the split tensile test result.

Table 3.5: Comparative study of results of hardened concrete of this work (laboratory) with models of other researchers.

Compressive Strength (average observed values) (N/mm^2) at 28 days	Split tensile strength in N/mm^2					
	Average observed value	Lavanya & Jegan (2015) $f_{t1}=0.249f_{ck}^{0.772}$	ACI Committee 318(2014) $f_{t2}=0.56f_{ck}^{0.5}$	Anoglu et al (2006) $f_{t3}=0.387f_{ck}^{0.63}$	CEB-FIB (1991) $f_{t4}=0.3f_{ck}^{0.66}$	Gardner (1990) $f_{t5}=0.33f_{ck}^{0.667}$
44.89	4.38	4.70	3.75	4.25	3.70	4.17
53.87	5.26	5.41	4.11	4.77	4.17	4.71
62.85	6.13	6.09	4.44	5.26	4.61	5.22

Table 3.6: Statistical analysis of the results of this work (laboratory) and the output of models of other researchers.

	The ratios of split tensile strength of this work and the existing models				
	Mean	Standard deviation	Maximum	Minimum	Maximum-Minimum
This work	5.2567	0.87500	6.13	4.38	1.75
Lavanya & Jegan (2015)	5.4000	0.69505	6.09	4.70	1.39
ACI Committee 318(2014)	4.1000	0.34511	4.44	3.75	0.69
Anoglu et al (2006)	4.7600	0.50507	5.26	4.25	1.01
CEB-FIB (1991)	4.1600	0.45508	4.61	3.70	0.91
Gardner (1990)	4.7000	0.52507	5.22	4.17	1.05

The comparative results of Table 5 and 6 show that the output of laboratory work of this study shows a good agreement with published work of other authors. The split tensile strength is important because it a function of the initiation time utilized in this work hence its accuracy validation.

v) The critical penetration depth

The critical penetration depth is essential in calculating the initiation time of corrosion. Table 3.7 shows the parametric study of the critical penetration depth from Equations,19,20 and 21.

Table 3.7 Parametric study of the critical penetration depth by different models

Sample Identity Characteristic strength and cover		Compressive strength(f_{cu}) (N/mm^2)	Tensile strength(f_t) (N/mm^2)	Critical penetration depth mm Rodriguez et al.	Torres-Acosta & Sagues	Xu and Shayan
25	70mm	44.89	4.38	0.0366	0.1190	0.8817
N/mm^2	60mm			0.0292	0.0961	0.7714
	45mm			0.0181	0.0661	0.6061
30	70mm	53.87	5.26	0.0167	0.119	0.9946
N/mm^2	60mm			0.0093	0.0961	0.8703
	45mm			-0.0018	0.0661	0.6838
35	70mm	62.85	6.13	-0.0029	0.1190	1.125
N/mm^2	60mm			-0.010	0.0961	0.9844
	45mm			-0.0214	0.0661	0.7735

From the results of Table 3.7, it can be noted that in all the models the critical penetration depth decreases with decrease in concrete cover. This is due to less resistance of samples with smaller covers for the same tensile strength. The Torres-Acosta and Sagues model has no variation in the strength of concrete. It is also noted that in the Rodriguez et al. model, the critical penetration depth tends to below zero for concrete strength of $30N/mm^2$ and $35N/mm^2$.This is due to non-consideration of the mechanical properties which affect the resistance of the concrete to cracking. The Xu and Shayan model considers the variants considered in this work and has been adopted in calculation of the initial corrosion period.

3.5 Results from Accelerated Corrosion Tests

3.5.1 Results from this work and from other researchers.

For this work Equation 3 was used to calculate the rate of corrosion (mm/year) inserted in equation 2 for the current density from the measured time for evolution of the maximum of the crack width of 0.2mm. The values shown in Table 3.8 were used to determine the equilibrium potential in Equation 11.

Table 3.8:Adopted values for determination of equilibrium potential(E_{corr})

Parameter	Value	Reference source
$C(t=0)$	$0.005kg/m^3$	Ba˘zant, 1979a [67]
$C_O(t=0)$	$8.576\ x\ 10^3 kg/m^3$	
E_{oa}	-3V	Applied Voltage
i_{oa}	3.75 x 10^{-4}µA/cm^2	Kranc, S., and Sag¨u´es, A. [68]
i_{oc}	1.25 x 10^{-5}µA/cm^2	
E_{oc}	3 V	Applied voltage

β_a	0.57 V	Calculated for an equivalent corrosion period
β_c	0.42 V	
E_{corr}	-1.52 V	From equation 11
i_a	14.71 µA/cm^2	From equation 8
V_{corr}	0.1705 mm/year	

T_1 is calculated from Equation 22 by converting to an equivalent rate of corrosion subsequently and subtracting from the duration of the test samples for propagation period applied in Vu and Stewart [33] and Li(2004a) [34] shown in table 3.8. Table 3.9 shows the critical penetration depth and current density for different samples.

$T_1(\text{years}) = \frac{x_{crit}(\text{mm})}{0.0116 I_{corr} \alpha(\mu A/cm^2)}$ and T_2=Total corrosion time –T_1

Table 3.9: The critical penetration depth and current density of samples tested.

Sample Identity		Cover (mm)	Mass of steel sample (gms)		Loss in weight (gms) measured	Critical penetration depth X_{crit} (mm)	Duration in days		Corrosion current density (µA/cm^2)		
			before corrosion	after corrosion			T_1	T_2	This work	Vu and Stewart (2000)	Li(2004a)
25 N/mm^2	150mm diameter	70	371	360.4	10.6	0.8817	19	88	0.691	1.86	0.606
	130mm diameter	60	371	362.3	8.7	0.7714	16	70	0.729	2.204	0.520
	100mm diameter	45	371	363.2	7.8	0.6061	14	62	0.766	2.204	0.473
30 N/mm^2	150mm diameter	70	371	361.5	9.5	0.9946	21	135	0.388	1.419	0.766
	130mm diameter	60	371	362.4	8.6	0.8703	19	123	0.303	1.674	0.729
	100mm diameter	45	371	363.4	7.6	0.6838	15	112	0.312	2.243	0.691
35 N/mm^2	150mm diameter	70	371	361.6	9.4	1.125	24	162	0.237	1.164	0.833
	130mm diameter	60	371	362.4	8.6	0.9844	21	151	0.237	1.637	0.804
	100mm diameter	45	371	363.1	7.9	0.7735	17	141	0.227	1.836	0.785

Fig.3.5 shows the relationship between corrosion current density against reinforcement cover and propagation period from Table 3.9.

British Journal of Civil and Architecture Engineering
ISSN: 2232-8232
Volume 02, Issue 06, June, 2020

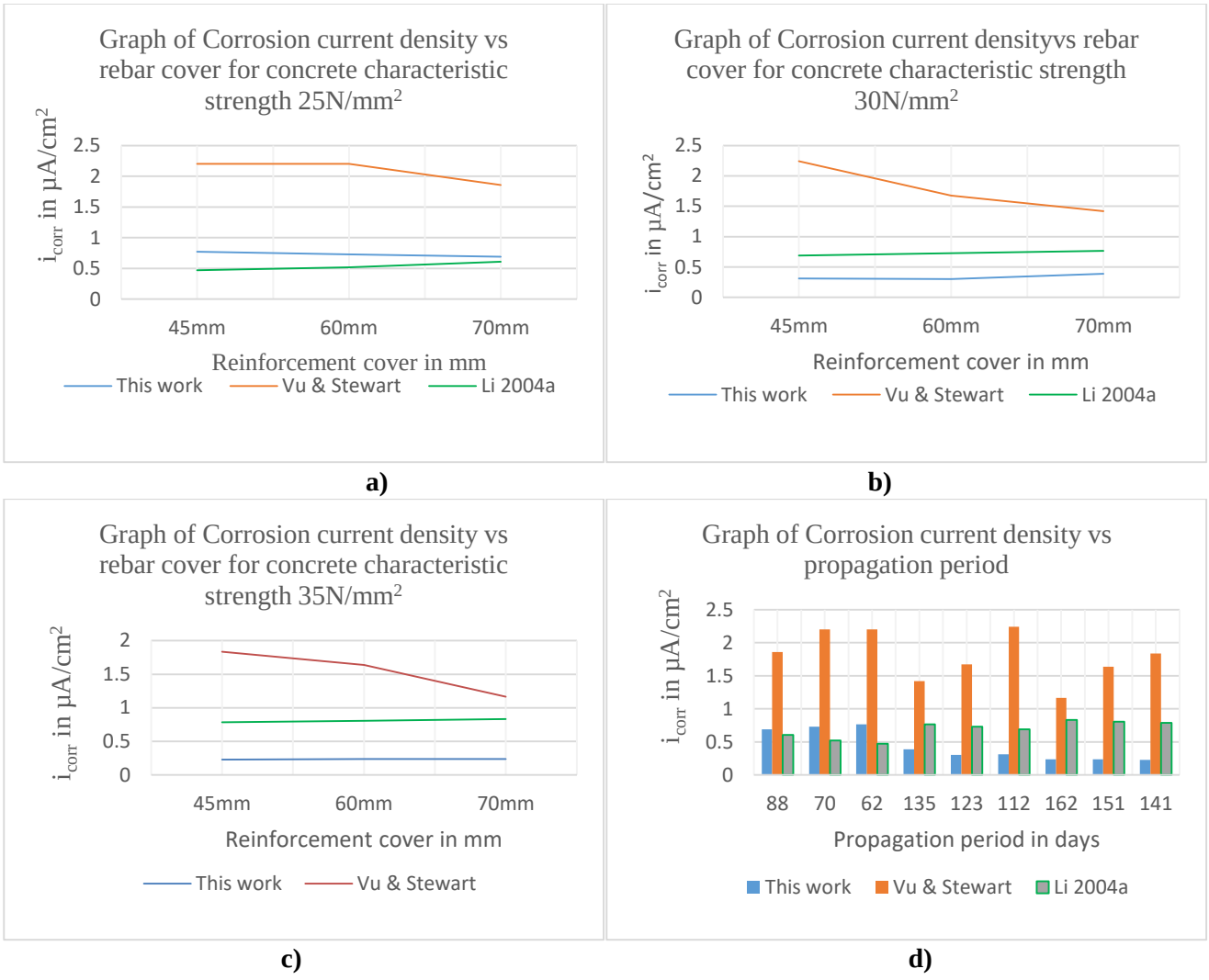


Figure 3.5: a)-c) Graph of Current density vs reinforcement cover for 25N/mm^2,30N/mm^2 and 35N/mm^2 and d) propagation period

From Fig. 3.5 graph a)-c), its noted that the corrosion current density generally decreased with an increase in reinforcement cover in this work and the Vu and Stewart model in all concrete strengths considered. Corrosion current density depends on physical, electromechanical and mechanical processes where the cover thickness plays an important role. In the Li 2004a model the corrosion current density increases with an increase in concrete cover within the same concrete strength but remains constant for the same cover in different strengths. The Li 2004a model considers only the corrosion duration and neglects any other factor. From Fig.3.5 d), it can be noted that the corrosion current density decreased with increase in propagation period in this study and in the Vu and Stewart. As the current density increases the rust expansion over the bar increases with a decrease in propagation period.

Fig.3.6 shows the relationship between the critical penetration depth and the corrosion current density of this work and selected models.

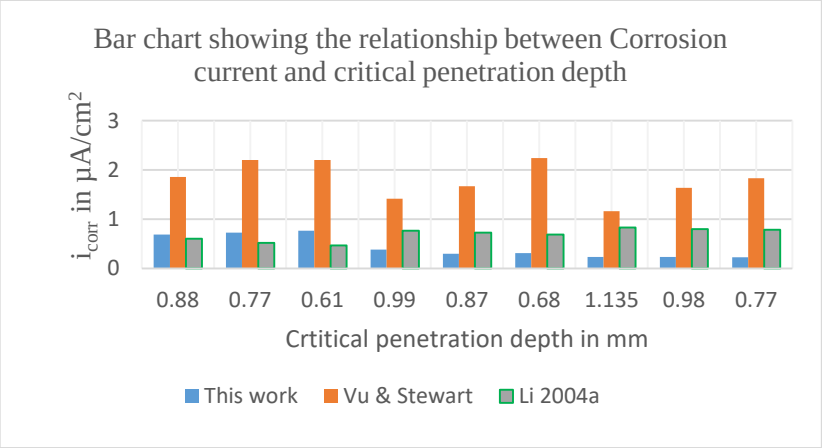


Figure 3.6: Relationship between the critical penetration depth and the corrosion current density of this work and selected models.

From Fig.3.6, the corrosion current density by Vu and Stewart is more than twice the results of this work. This is because not all factors affecting the corrosion rate are considered. In the Li 2004a model the corrosion current density decreases with decrease in critical penetration depth contrary to the results of this work. This model considers the corrosion period as the only factor influencing the corrosion current density, the influence of more factors may influence the results.

Fig.3.7 shows the relationship between corrosion current density and reinforcement mass loss for a crack width of 0.2mm

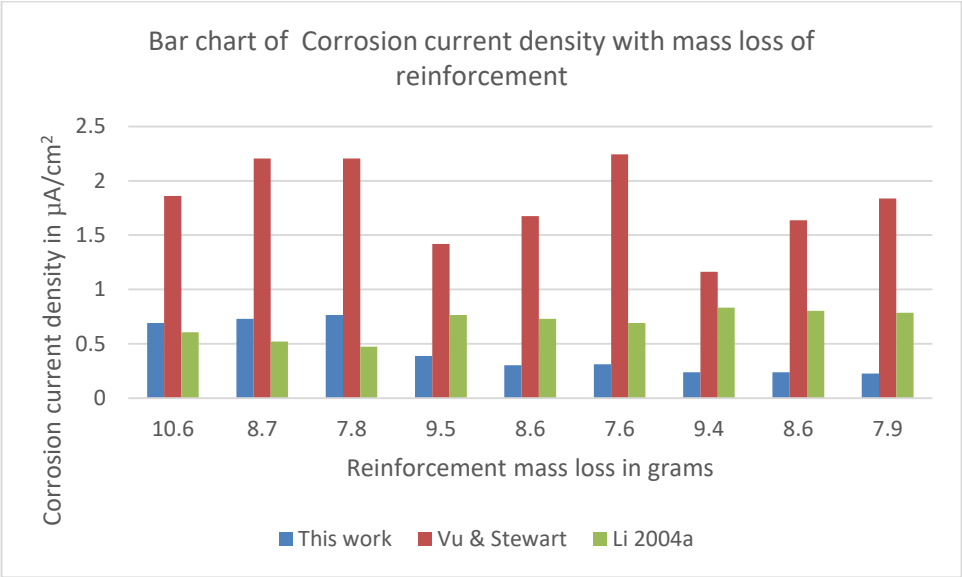


Figure 3.7 Relationship between corrosion current density and reinforcement mass loss for a crack width of 0.2mm

From Fig.3.7, the corrosion current density by Vu and Stewart increases with decrease in reinforcement mass loss and is contrary to the results of this work and the Li 2004a model. Other than the corrosion period, the water cement ratio and the concrete cover, the mechanical properties of the concrete may influence the rate of corrosion current density and reinforcement mass loss.

The correlation of the result of this work and those of the Vu and Stewart (2000) model have been used for generation of the proposed current density model for the propagation period for this study.

3.5.2 Statistical relationship of the result of this work and those of Vu and Stewart (2000).

Table 9 shows the correlation of the result of this work and those of Vu and Stewart (2000)

Table 3.9: Correlations of the results of this work and those of Vu and Stewart

			This work	Vu & Stewart
Kendall's	This work	Correlation Coefficient	1.000	0.400
		Sig. (2-tailed)	0.000	0.140
	Vu Stewart	&Correlation Coefficient	0.400	1.000
		Sig. (2-tailed)	0.140	0.000
Spearman's rho	This work	Correlation Coefficient	1.000	0.546
		Sig. (2-tailed)	0.000	0.128
	Vu stewart	&Correlation Coefficient	0.546	1.000
		Sig. (2-tailed)	0.128	0.000

From Table 3.9, the result of this work has no significantly correlation with the results of Vu and Stewart model. A modified Vu and Stewart model is proposed for this work.

3.5.3 Proposed model for this work

Fig.3.8 shows a Graph for the relationship between this work and the Vu and Stewart model.

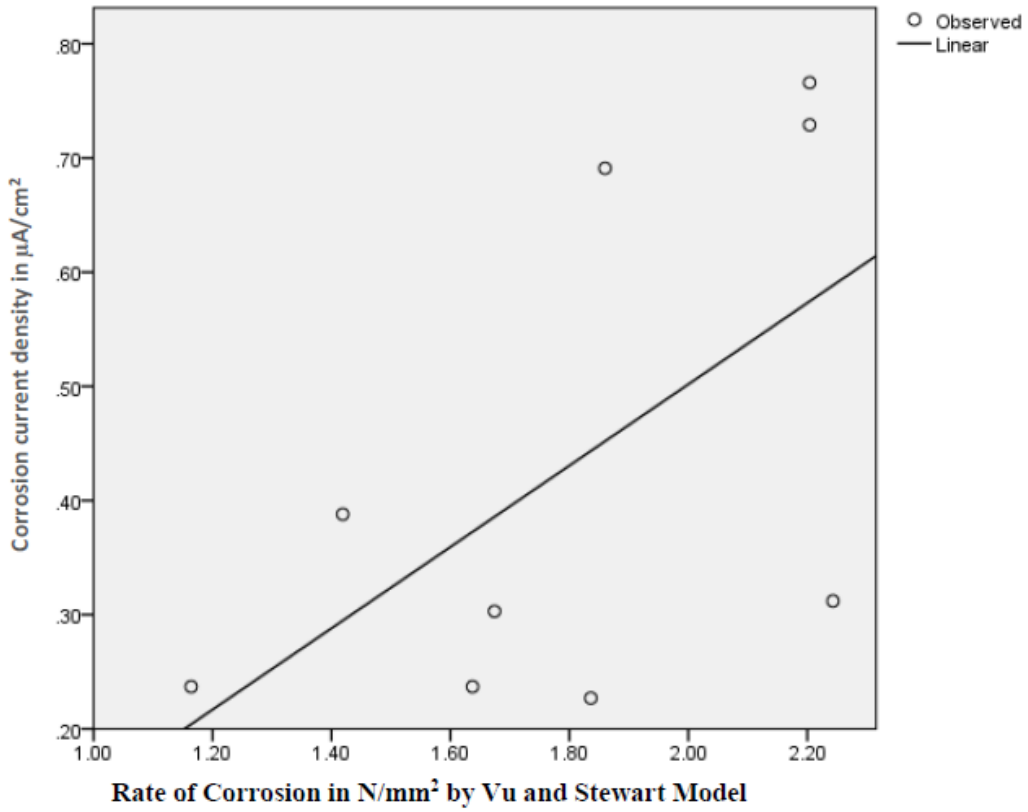


Figure 3.8: Relationship of the results of this work and those of Vu and Stewart (2000)

From Fig.3.8, a coefficient of 0.356, standard error of 0.028, Table 3.10 shows the statistical comparison between the output of this work, the Vu and Stewart (2000) and the proposed model.

Table 3.10: Statistical Relationship between the results of this work, the Vu model and the proposed model

	Mean difference	Std	Std. Error Mean	Sig. (2-tailed)	95% Confidence Interval	
					Lower	Upper
This work	0.4322	0.22855	0.07618	0.010	0.2565	0.6079
Vu and Stewart	1.8046	0.37408	0.12469	0.001	1.5170	2.0921
Proposed model	0.6411	0.13299	0.04433	0.001	0.5389	0.7433

From table 3.10, the proposed model output for this work compares well with the output of this research and therefore the corrosion current density can be obtained from equation 34:

$$i_{corr}(t_2) = \left[13.46\,(1 - {}^{w}/_{c})^{-1.64}(1 + t_2)^{\frac{-1}{3}}\right] / d \qquad (\mu A/cm^2) \qquad 34)$$

3.5.3 Proposed service Life model of reinforced concrete water conveyancing structures

a) Crack Initiation Period (T_1) and propagation (T_2)

This is the time to first visible crack and is obtained from Equation 35;

$$T_1 = \left(\frac{f_t(c+d)(1+v)}{E_{eff}d\beta}\right) x\ 10^{-3}\ x\left(0.0116 I_{corr}\ (\frac{\mu A}{cm^2})\right)^{-1} (\text{years}) \qquad 35)$$

The propagation period from experimental work was obtained from total period for 0.2mm crack evolution minus crack initiation period(T_1).

b) Crack propagation Period (T_2)

Equation 36 is proposed for calculation of T_2 in days and compared with the experimental results and models of others researches as shown in table 3.11.

$$T_2 = \left[\rho_{rust}\left(L\,\pi\left[\frac{Cf_t}{E_{ef}}\left(\frac{a^2+b^2}{b^2-a^2} + v_c\right) + t_1\right]d + \frac{M_{st}}{\rho_{st}}\right)\right]^2 \frac{4.9691\alpha}{di_{corr}} + \left[\left(\frac{\omega-0.05}{\beta} + x_{crit}\right)\frac{f_t}{0.07192 i_{corr} k}\right] \qquad 36)$$

T_2 can be defined into two levels;

$T_2 = T_{p1} + T_{p2}$

$$T_{p1} = \left[\rho_{rust}\left(L\,\pi\left[\frac{Cf_t}{E_{ef}}\left(\frac{a^2+b^2}{b^2-a^2} + v_c\right) + t_1\right]d + \frac{M_{st}}{\rho_{st}}\right)\right]^2 \frac{5.846\alpha}{di_{corr}} \qquad 37)$$

$$T_{p2} = \left[\left(\frac{\omega-0.05}{\beta} + x_{crit}\right)\frac{f_t}{0.07192 i_{corr} k}\right] \qquad 38)$$

Where

L =reinforcement length exposed to corrosion(cm)

C= Concrete cover in cm

ω =characteristic crack width taken as 0.2mm

x_{crit}=critical penetration depth (mm)

β= Coefficient taken as 0.01125

t_1 =0.002 cm

$\rho_{rust} = 3.6$ g/cm^3

v_c = Concrete poison's ratio taken as 0.2

E_{eff} =effective elastic modulus=E/(1+ϕ) (N/mm^2)

E =Elastic modulus (N/mm^2)

ϕ = concrete creep coefficient

k = Current density factor taken as 10.

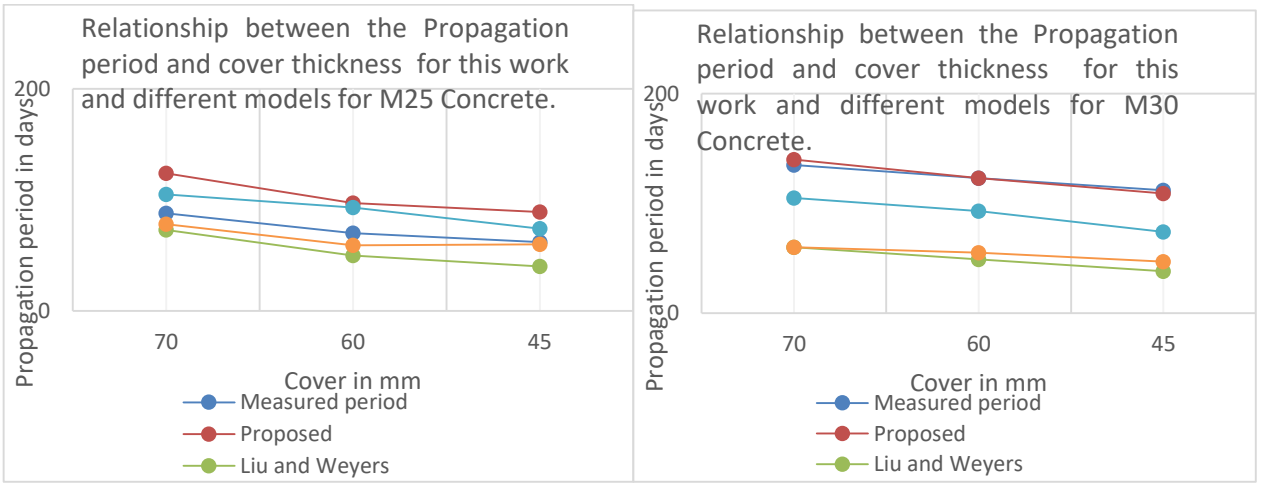
British Journal of Civil and Architecture Engineering
ISSN: 2232-8232
Volume 02, Issue 06, June, 2020

f_t = Concrete tensile strength (N/mm^2)
α= relation between atomic weight of iron (55.8) and the molecular weight of the rust product taken as 0.523.
a = the inner radius [(d+2t$_1$)/2] (cm)
b = the outer radius [C+(d+2t$_1$)/2] (cm)

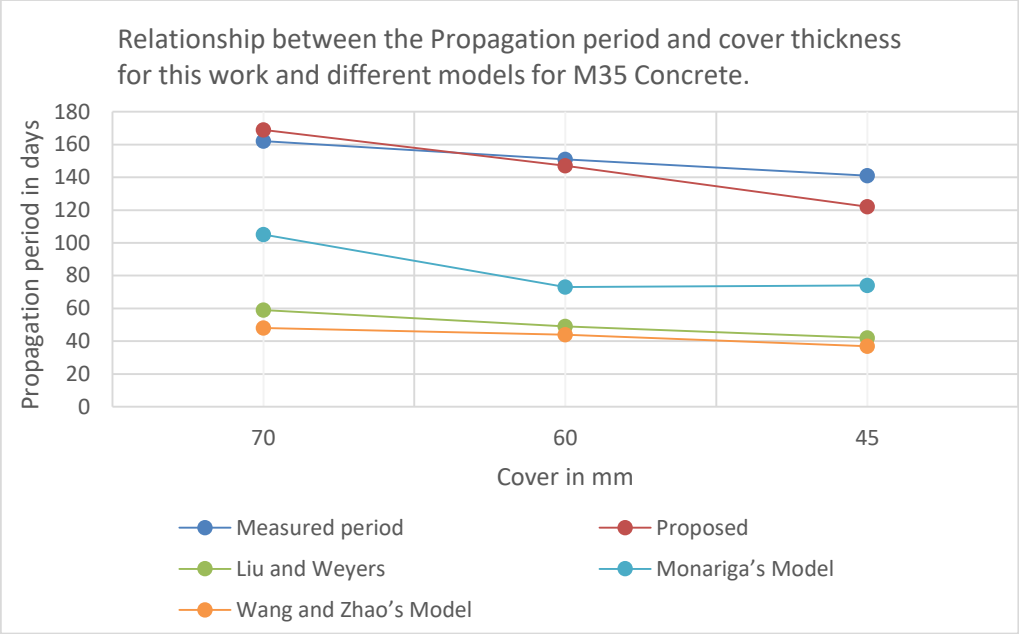
Table 3.11shows a parametric study of the propagation period of experimental work with a proposed model and models of other researchers.

Sample Identity		Reinforcement cover in mm	Mass loss of steel sample after corrosion (gms)	T_2 days				
				Measured period	Proposed Model	Liu and Weyers Model	Monariga's Model	Wang and Zhao's Mod
25 N/mm^2	150mm diameter	70	10.6	88	124	73	105	78
	130mm diameter	60	8.7	70	97	50	93	59
	100mm diameter	45	7.8	62	89	40	74	60
30 N/mm^2	150mm diameter	70	9.5	135	140	60	105	60
	130mm diameter	60	8.6	123	123	49	93	55
	100mm diameter	45	7.6	112	109	38	74	47
35 N/mm^2	150mm diameter	70	9.4	162	169	59	105	48
	130mm diameter	60	8.6	151	147	49	73	44
	100mm diameter	45	7.9	141	122	42	74	37

Figure 3.8 shows the relationship between the reinforcement cover and the propagation period results of this work, the proposed model and the results of other models as shown in Table 3.11.



a) **b)**



c)

Figure 3.8: Graph a)-c) Relationship between the reinforcement cover and the propagation period results of this work, the proposed model and the results of other models as shown in table 3.11

From Table 3.11 and Figure 3.8, the propagation period reduced with reduction of concrete cover and strength in the study results and all models considered. This is because it takes a shorter period for chloride ions to percolate from the surface to the reinforcement bar in a smaller cover and the contrary is true for larger covers. In stronger concrete samples, the voids are more compressed reducing the rate of percolation of the aggressive chloride ions responsible for corrosion. The proposed model has a high correlation with the results of this work comparable to the other models considered. This is because after crack initiation considered approximately 0.05mm, the models have not

3.5.4 Application and limitation of the proposed model.

Figure 3.9 shows the procedure to estimate the corrosion points of initiation and propagation points for service life prediction.

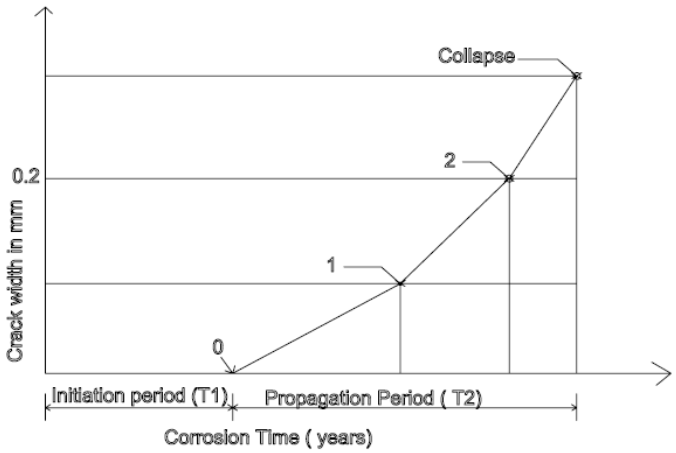


Figure 3.9: Corrosion initiation and propagation points.

Point 0: is the initiation period calculated from Equation 35 and is associated with lose of the passivation layer.
Point 1: is the propagation period calculated using Tp_1 and is related to crack with of approximately 0.5mm.
Point 2: is the propagation period calculated using T_{p2} and is related to crack expansion for maximum acceptable width.
This model is limited for use for water conveyancing structures.

4.0 Conclusion

From the results of this research, the following conclusions can be drawn;

- The rate of corrosion is affected by the compressive strength, split tensile strength and reinforcement cover.
- Li(2004a) model does not correlate with the results of this work and those of Vu and Stewart (2000) model.
- A service life model for water conveyancing structures has been proposed taking account of the initiation and propagation period.

5. References

[1] Bolzoni, F., Coppola, L., Goidanich, S., Lazzari, L., Ormellese, M., and Pedeferri, M. P. (2004), "Corrosion inhibitors in reinforced concrete structures," Part 1: Preventative technique. Corrosion Engineering, Science and Technology, 39(3), 219-228.

[2] Lee, S. K., Krauss, P. D., and Virmani, Y. P. (2005), "Resisting corrosion," Public Roads, 68(6), 58-63.

[3] Xu J., Jiang L. and Wang Q. (2009), "Finite element model of reinforcement corrosion in concrete," Water Science and Engineering, 2(2), 71-78.

[4] Talbot D., Talbot J. (1998), "Corrosion Science and Technology," CRC Press, London.

[5] Bertolini L., Elsener B., Pedeferri P. and Polder R. (2004), "Corrosion of Steel in Concrete," Wiley.

[6] ACI Committee 222(2005), Protection of metals in concrete against corrosion, ACI 222R-01, ACI Manual of Concrete Practice.

[7] Torres-Acosta, A. A., Navarro-Gutierez, S. and Teran-Guillen. (2007), "Residual flexure capacity of corroded reinforced concrete beams," Engineering Structures, 29, 1145–1152.

[8] Zhang, R., Castel, A. and Francois, R. (2009), "Serviceability limit state criteria based on steel–concrete bond loss for corroded reinforced concrete in chloride environment," Materials and Structures.

[9] Torres-Acosta, A. A., Fabela-Gallegos, M. J., Munoz-Noval, A., Vazques-Vega, D. and Hernandez-Jimenez, J. R. (2004), "Influence of corrosion on the structural stiffness of reinforced concrete beams,"Corrosion. 60(9): 862-872.

[10] Malumbela, G., Alexander, M. and Moyo, P. (2009b), "Steel corrosion of RC structures under sustained service loads – a critical review," Engineering Structures. 31: 2518-2525.

[11] Liu Y. and Weyers, R.E. (1998), "Modeling the Time-to-Corrosion Cracking in Chloride Contaminated Reinforced Concrete Structures," ACI Materials Journal. 95(6): 675-681.

[12] El Maaddaway, T. and Soudki K. (2007), "A model for prediction of time from corrosion initiation to corrosion Cracking," Cement and Concrete Composites. 29(3): 168-175.

[13] Andrade, C., and Alonso, C. (1996a), "Durability design based on models for corrosion rates," In H. Jennings, J. Kropp, and K. Scrivener (Eds.), The Modelling of Microstructure and Its Potential for Studying Transport Properties and Durability (pp. 473–492). The Netherlands: Kluwer Academic Publishers.

[14] Andrade, C., and Alonso, C. (1996b), "Progress on design and residual life calculation with regard to rebar corrosion of reinforced concrete," In N. Berke, E. Escalante, C. Nmai,and D. Whiting (Eds.), Techniques to Assess the Corrosion Activity of Steel Reinforced Concrete Structures, ASTM STP 1276 (pp. 23–40).

[15] Rodriguez, J., Ortega, L., Casal, J., and Diez, J. (1996), "Corrosion of reinforcement and service life of concrete structures," In C. Sj¨ostr¨om (Ed.), Durability of Building Materials and Components, 7 (1),117–126).

[16] Tran, K., Nakamura, H., Kawamura, K., Kunieda, M. (2011), "Analysis of crack propagation due to rebar corrosion using RBSM," Cement Concrete Comp,33:906-17.

[17] Toongoenthong, K., Maekawa, K. (2005), "Simulation of coupled corrosive product formation, migration into crack and propagation in reinforced concrete," J Adv Concr Technol,3(2):253-65.

[18] Liu, Y., Weyers, R.E. (1998), "Modeling the time-to-corrosion cracking in chloride contaminated reinforced concrete structures," ACI Mater J.,95(6):675-80.

[19] Luković, M., Pacheco, J., Schlangen,E. (2013), "Cracking of the concrete cover due to reinforcement corrosion: A two-dimensional lattice model studyJuly,"Construction and Building Materials, 44:626–638.

[20] Wong, H., Zhao, Y.X., Karimi, A.R., Buenfeld, N.R., Jin, W.L. (2010), "On the penetration of corrosion products from reinforcing steel into concrete due to chloride-induced corrosion," Corros Sci.,52:2469-80.

[21] Martín-Peréz B. (1999), "Service life modelling of R.C. highway srtuctures exposed to chlorides," Toronto: University of Toronto.

[22] Balafas, I., Burgoyne, C.J. (2011), "Modeling the structural effects of rust in concrete cover," J Eng Mech-ASCE,137(3):175-85.

[23] Pantazopoulou, S., Papoulia, K.D. (2001), "Modeling cover-cracking due to reinforcement corrosion in RC structures," J Eng Mech-ASCE,27(4):342-51.

[24] Duracrete (2000), "Probabilistic Performance based Durability Design of Concrete Structures,"The European Union–Brite EuRam III, BE95-1347/R17, CUR, Gouda, The Netherlands.

[25] RILEM TC 154-EMC (2003), "Electrochemical Techniques for Measuring Metallic Corrosion," Materials and Structures / Matériaux et Constructions, 37, 623-643.

[26] Ahmad S. (2003), "Reinforcement corrosion in concrete structures, its monitoring and service life prediction: A Review," Cement and Concrete Composites, 25(4-5), 459-471.

[27] Montemor, M. F., Simoes, A. M. P., and Salta, M. M. (2000), "Effect of fly ash on concrete reinforcement corrosion studied by EIS," Cement and Concrete Composites,22(3), 175-185.

[28] Sathiyanarayanan, S., Natarajan, P., Saravanan, K., Srinivasan, S., and Venkatachari, G. (2006), "Corrosion monitoring of steel in concrete by galvanostatic pulse technique," Cement and Concrete Composites,28(7), 630-637.

[29] Andrade, C., and Alonso, C. (2004), "Test methods for on-site corrosion rate measurement of steel reinforcement in concrete by means of the polarization resistance method," Materials and Structures, 37(9), 623-643.

[30] Nikunj N. S. Vanpariya K. (2019), "Evaluation of corrosion rate in steel reinforcement of RCC," International Research Journal of Engineering and Technology, 6(11),1030-1034.

[31] RILEM TC 154-EMC (2003), "Electrochemical Techniques for Measuring Metallic Corrosion' Materials and Structures / Matériaux et Constructions," 36,461-471

[32] Yalcyn, H., and Ergun, M. (1996), "The prediction of corrosion rates of reinforcing steels in Concrete," Cement and Concrete Research, 26(10), 1593–1599.

[33] Vu, K.A.T. & Stewart, M.G. (2000), 'Structural reliability of concrete bridges including improved chloride-induced corrosion models," Structural Safety, 22(4), 313-333.

[34] Li, C.Q. (2004a), "Reliability based service life prediction of corrosion affected concrete structures," Journal of Structural Engineering 130(10), 1570–1577.

[35] Tuutti, K. 1982, Corrosion of Steel in Concrete, Swedish Cement and Concrete Research Institute, Fo 4.82, Stockholm.

[36] Rasheeduzzafar, Dakhil, F. H., Bader, M. A., & Mukarram Khan, M. (1992). "Performance of Corrosion-Resisting Steels in Chloride-Bearing Concrete," ACI Materials Journal,Vol. 89, No. 5, pp. 439-448.

[37] State of the art- Modelling of reinforcement corrosion in concrete. Coin Project Report 7 - 2008

[38] Shayan, A., Xu, A. (2016), "Relationship between Reinforcing Bar Corrosion and Concrete Cracking," Aci Materials Journal 113(1).

[39] Torres-Acosta, A. A., & Sagues, A. A. (2004). "Concrete Cracking by Localized Steel Corrosion--Geometric Effects," ACI Materials Journal,101(6), 501-507

[40] El Hajj, Peter. (2015). Probabilistic Modelling of Multiphasic Degradations for Maintenance Optimization of Infrastructures in Civil Engineering. Thesis for: Doctor of Philosophy in Civil Engineering

[41] Teplý B., Vorechovská, D.)2012), "Limit states, reliability and modelling,"Journal of Advanced Concrete Technology, 10(11).

[42] Andrade., Alonso, C. (1996), "Corrosion rate monitoring in the laboratory and on-site," Construction and Building Materials, 10(5), 315-328

[43] Andrade, C., Sanchez, J, Fullea, J., Rebolledo, N., Tavare, S. F. (2012) On-site corrosion rate measurements:3D simulation and representative values. Mater Corros 63(12):1154–1164

[44] Andrade, C. (2017), "Reliability analysis of corrosion onset: initiation limit state," J Struct Integr Maint 2(4):200–208

[45] Bazant, Z. (1979b). Physical model for steel corrosion in concrete sea structures—application. Journal of the Structural Division, 105(ST6), 1155–1166.

[46] Scrivener, K.L., Crumbie, A.K., Laugesen, P. (2000), "The interfacial transition zone (ITZ) between cement paste and aggregate in concrete," Interface Sci.,12(4):411-21.

[47] Shane, J.D., Mason, T.O., Jennings, H.M., Garboczi, E.J., Bentz, D.P. (2000), "Effect of the interfacial transition zone on the conductivity of portland cement mortars," J Am Ceram Soc.,83(5):1137-44.

[48] Yang, C.C. (2005), "Effect of the percolated interfacial transition zone on the chloride migration coefficient of cement-based materials," Mater Chem Phys.,91(2-3):538-44.

[49] Morinaga,S. (1989), "Prediction of Service Lives of Reinforced Concrete Buildings Based on Rate of Corrosion of Reinforcing Steel," Special report of the institute of Technology, Japan, Skimiza Corporation.

[50] Wang, X.M., Zhao, H.Y., 1993. The residual service life prediction of RC structures. In: Nagataki, S. (Ed.), Durability of Building Materials and Components, 6, 1107–1114.

[51] Jones A. (2008) Eurocode 2 – Design of concrete structures: Part 3. Liquid-retaining and Containment Structures. Dissemination of information workshop, Brussels February 2008.

[52] Kenya Bureau of Standards,KS EAS 18-1:2001-Cement Part 1:Composition, Specification and Conformity Criteria for Common Cements. Kenya Bureau of Standards, Nairobi,2005.

[53] Kumbhar, P.D. and Murnal, P.B. (2012), "Assessment of Suitability of Existing Mix Design Methods of Normal Concrete for Designing High Performance Concrete," International Journal of Civil and Structural Engineering, 3,158-167.

[54] Neville M. (1996). "Properties of Concrete," Pitman Publishing Company," London, UK.
[55] Neville A.M., Brooks J.J. (2012). "Concrete Technology," Longman, London, UK.

[56] Shetty M. S. Concrete Technology Theory and Practice S. Chand & Company Ltd. Ram Nagar, New Delhi.

[57] Neville A. M. (2011), Properties of Concrete, 5th edition. Pearson Education Limited.

[58] Arum gam, B. (2014), "Effect of Specific Gravity on Aggregate Varies the Weight of Concrete Cube," International Journal of Civil Engineering, 1(3),1-9.

[59] British Standard Institutes, BS EN 1097-6:2000, Tests for mechanical and physical properties of aggregates. Determination of particle density and water absorption, British Standard Institution, London

[60] British Standard Institutes, BS 882:1992, Specification for aggregates from natural sources for concrete

[61] British Standard Institutes, BS 8007:1987, Code of practice for the design of concrete structures for retaining aqueous liquids

[62] Zerdi A.T. (2014). Strength Exhibition of M25 Grade Concrete with Limestone Quarry Dust Utilization for Fine Aggregates, Global Journal of Research Analysis International,5(1).

[63] ASTM C117, "Standard Test Method for Materials finer that 75-um (No. 200) sieve in mineral aggregates by washing." American Society for Testing and Materials, 1995.

[64] BS 882; - Specification for aggregates from natural sources for concrete. British Standards Institute, London United Kingdom, 1992.

[65] ASTM C40, "Standard Test Method for effect of organic impurities in fine aggregates on strength of mortar," American Society for Testing and Materials ASTM International, 2004.

[66] KS EAS 18. Cement Standard - Part 1: Composition, Specifications and Conformity Criteria. KEBS, Kenya. 2001.

[67] Baˇzant, Z. (1979b)," Physical model for steel corrosion in concrete sea structures application," Journal of the Structural Division, 105(ST6), 1155–1166.

[68] Kranc, S., and Sag¨u´es, A. (1994), "Computation of reinforcing steel corrosion distribution in concrete marine bridge substructures," Corrosion, 50(1), 50–61.

This work is licensed under a Creative Commons Attribution Non-Commercial 4.0 International License.